Molecular Dynamics Simulation of Liquid Water: Hybrid Density Functionals†

Teodora Todorova,‡ Ari P. Seitsonen,‡ Jürg Hutter,*,‡ I-Feng W. Kuo,§ and Christopher J. Mundy§

Physical Chemistry Institute, University of Zurich, Winterthurerstrasse 190, CH-8057 Zurich, Switzerland, and Computational Chemical Biology, Chemistry, and Material Science L-367, Lawrence Livermore National Laboratory, Livermore, California 94550

Received: September 11, 2005; In Final Form: October 24, 2005

The structure, dynamical, and electronic properties of liquid water utilizing different hybrid density functionals were tested within the plane wave framework of first-principles molecular dynamics simulations. The computational approach, which employs modified functionals with short-ranged Hartree−Fock exchange, was first tested in calculations of the structural and bonding properties of the water dimer and cyclic water trimer. Liquid water simulations were performed at the state point of 350 K at the experimental density. Simulations included three different hybrid functionals, a meta-functional, four gradient-corrected functionals, and the local density and Hartree−Fock approximations. It is found that hybrid functionals are superior in reproducing the experimental structure and dynamical properties as measured by the radial distribution function and self-diffusion constant when compared to the pure density functionals. The local density and Hartree−Fock approximations show strongly over- and understructured liquids, respectively. Hydrogen bond analysis shows that the hybrid functionals give slightly smaller average numbers of hydrogen bonds than pure density functionals but similar hydrogen bond populations. The average molecular dipole moments in the liquid from the three hybrid functionals are lower than those of the corresponding pure density functionals.

1. Introduction

Water, although being the most abundant liquid on the planet, is certainly the least understood.[1,2] This is likely attributed to its anomalously high dipole moment and polarizability, in addition to its self-dissociation capability, which makes this liquid a challenge from the point of view of theory. One popular approach to simulating water is utilizing an interaction potential derived from the Kohn−Sham formulation[3] of density functional theory (KS-DFT). The accuracy of KS-DFT heavily relies on the definition of the exchange and correlation (XC) functional. The success of the generalized gradient approximation (GGA) (e.g., the combination of Becke's exchange[4] with the Lee, Yang, and Parr correlation[5] functional (BLYP) and the Perdew, Burke, and Ernzerhof (PBE) functional[6]) to the XC functional dramatically accelerated KS-DFT studies of liquid water. More recently, through the use of terascale computing and state-of-the-art electronic structure algorithms there have been many detailed studies of liquid water[7−14] significantly extending both the size and the length of the simulations compared to earlier studies,[15,16] showing that our basic understanding of liquid water as obtained from KS-DFT in conjunction with GGA XC functionals is far from complete. Moreover, results from simulations utilizing free boundary conditions and efficient sampling techniques[7,17−19] have indicated that there may be a significant dependence of structural and dynamic properties on the choice of thermodynamic state, namely, 1 g/cm^3 at 298 K and 1 atm pressure. In particular, in simulations where the state point is allowed to vary, results indicate that BLYP water may be less dense than the true liquid water. Nevertheless, the height of the first peak in the oxygen−oxygen radial distribution function (RDF) and the mean-square displacement (MSD) have been the most common analysis tools in the molecular dynamics calculations of water. A common conclusion has been that there is a degree of overstructuring of the first peak in the oxygen−oxygen RDF as compared to reconstructed RDFs based on experimental neutron diffraction data.[7−14] In addition, a low MSD, as compared to experiment, is found in all KS-DFT simulations of liquid water.

However, it should be pointed out that the cause and degree of overstructuring and slower diffusion are not universally agreed upon. Having said this, there seems to be a consensus that the first peak of the oxygen−oxygen RDF ranges from 3 to 3.5, subject to various simulation protocols such as choice of GGA functional, system size, and duration of simulation. Given that the accepted first peak of the oxygen−oxygen RDF is around 2.7 at 298 K and 1 atm, there has been speculation that the cause of this could be due to quantum effects.[9,10] However, a recent path-integral KS-DFT calculation reported in the literature points to this not being the case.[20] In light of recent simulation data and, more importantly, new experiments pointing to a re-interpretation of our conventional wisdom on the structure of the first solvation shell of liquid water, the need for more accurate and careful simulation studies is exceedingly important.[21−23]

Thus, the present study attempts to contribute to a systematic evaluation of exchange and correlation functionals on the structural and dynamic properties of liquid water. The importance of the exchange functional for an accurate description of water has been evident already from the first simulations[15,16] and has been confirmed in recent studies.[11,14,24] It is therefore natural that the performance of exchange functionals, including

† Part of the special issue "Michael L. Klein Festschrift".

* Author to whom correspondence should be addressed. Phone: +41-44-635-4491. Fax: +41-44-635-6838. E-mail: hutter@pci.unizh.ch.

‡ University of Zurich.

§ Lawrence Livermore National Laboratory.

10.1021/jp055127v CCC: $33.50
Published on Web 12/06/2005

hybrid functionals, is of special interest. Through the use of the terascale computing resources that are currently available at U. S. national laboratories, condensed-phase simulations of water utilizing hybrid functionals are now feasible. Because of the indications that BLYP water has a lower critical temperature and liquid densities than the corresponding experimental values,[7,17−19] we chose a state point at an elevated temperature of 350 K using the experimental density to compensate for the possible onset of glassy behavior.[11,13,14] The same temperature and density were employed for all functionals and the TIP4P reference calculation. The same procedure has been used in previous comparisons of functionals.[14,16] Thus, we present a study of three hybrid functionals in comparison to common GGAs, the local density and the Hartree−Fock approximations. The computational setup is tested on calculations of the water dimer and the cyclic water trimer. The performance of the functionals is evaluated for liquid water simulations at 350 K and at the experimental density using partial radial distribution functions, mean-square displacements, molecular dipole moments, and hydrogen bonding analysis.

2. Computational Details

The calculation of Hartree−Fock exchange within a plane wave framework has been achieved before.[25] Apart from a divergence for the zero wavevector case, the basic strategy for the implementation is straightforward[25,26] and utilizes a series of Fourier transforms for all pairs of occupied orbitals. The Hartree−Fock exchange energy can be calculated in reciprocal space

$$E_{\mathrm{HFX}} = -\frac{1}{4\Omega}\sum_{ij} f_i f_j \sum_{\mathbf{G}} \Phi(\mathbf{G})|C_{ij}(\mathbf{G})|^2 \qquad (1)$$

where $\Phi(\mathbf{G})$ is the Green's function appropriate for the chosen boundary conditions, f_i, f_j are occupation numbers, and $C_{ij}(\mathbf{G})$ are the expansion coefficients of the overlap density for orbitals i and j in reciprocal space. The divergence does not appear for $\Phi(\mathbf{G})$ in the case of isolated systems (see ref 27 for an overview of methods) but needs special care for periodic boundary conditions. A solution was presented by Gygi and Baldereschi,[25] and the same method was also used in the recent implementation of exact exchange in a projector augmented wave formalism.[28] An alternative approach is to use a uniform background charge to compensate for the divergence. This route was taken by Chawla and Voth[26] and Bernasconi et al.[29] in connection with a time-dependent DFT calculation. In the current work we use a screened Coulomb operator of the form $erfc(\alpha r)/r$ that also avoids the divergence. This approach is in the spirit of recent functional developments[30] that only include short-ranged Hartree−Fock exchange into hybrid functionals, thereby allowing significant savings in computer time for localized basis set calculations. However, in a plane wave environment no immediate savings in computer time are possible with this approach. On the basis of the work of Heyd et al.,[30] we assume that the screened exchange can also be used in standard hybrid functionals without too much loss of accuracy. The definition of functionals used in this study is given in Table 1. Although these definitions depart from the original settings, we will still use the common acronyms for the functionals.

Computational efficiency is a major concern in exact exchange calculations using plane waves. Calculation of the wave function forces by applying the exact exchange operator to all orbitals requires N^2 (N is the number of orbitals) Fourier transforms of single orbitals as well as orbital pair densities.

TABLE 1: Definition of Exchange−Correlation Functionals Used in This Study[a]

abbreviations	definition
LDA	E_{xc}[Pade]
BLYP	E_x[B88] + E_c[LYP]
XLYP[53]	E_x[Slater] + 0.722 ΔE_x[B88] + 0.347 ΔE_x[PW] + E_c[LYP]
PBE	E_x[PBE] + E_c[PBE]
rPBE	E_x[rPBE] + E_c[PBE]
TPSS	E_{xc}[TPSS]
B3LYP[54]	0.80E_x[Slater] + 0.72ΔE_x[B88] + 0.20E[HFXS] + E_c[PZ] + 0.81ΔE_c[LYP]
X3LYP[53]	0.782E_x[Slater] + 0.542ΔE_x[B88] + 0.218E[HFXS] + 0.167ΔE_x[PW] + E_c[PZ] + 0.871ΔE_c[LYP]
PBE0[55]	0.75E_x[PBE] + 0.25E[HFXS] + E_c[PBE]
HF	E[HFXS]

[a] B3LYP and X3LYP have a slightly different definition from other implementations. Exact exchange contributions are always replaced by a screened Hartree−Fock exchange E[HFXS] formula (see text for more information). $E_x[\mathrm{Slater}] = -(3/2)((3/4\pi))^{1/3}\sum_\sigma \int \rho_\sigma(r)^{4/3}\,dr$. ΔE_x refers to the corresponding gradient-corrected functional with E_x[Slater] subtracted. ΔE_c[LYP] denotes the part of the LYP functional that depends on the density gradient. Fractional values of different exchange and correlation functionals were chosen based on a least-squares fitting to properties of a selected set of atoms and/or molecules, as described in the cited references: E_{xc}[Pade], ref 56; E_x[B88], ref 4; E_c[LYP], ref 5; E_x[PW], ref 57; E_x[PBE] and E_c[PBE], ref 6; E_x[rPBE], ref 58; E_c[PZ], ref 59; E_{xc}[TPSS], ref 60.

We avoid one of these transforms by keeping the orbitals in their real space representation in memory. A further important reduction in computer time can be achieved by an approximate representation of the orbital pair densities. As for the full electronic density, the pair densities are exactly represented by a plane wave expansion with a 4-fold increased kinetic energy cutoff compared to the orbital expansion. Reducing the cutoff for the pair densities to 2 times the orbital cutoff did not affect results for the water clusters and was used throughout all calculations in this study. Without loss of accuracy, we were able to increase parallel efficiency of the calculations by reducing the representation of data to 32 bit in the communication step of the three-dimensional fast Fourier transforms. The combination of these measures resulted in a more than 4-fold reduction of the total computer time needed.

It is common practice to apply pseudopotentials in plane wave calculations that have been generated with the same density functional from atomic reference systems. In this study we use norm-conserving pseudopotentials according to the scheme devised by Troullier and Martins[31] that allow for a comparably low wave function cutoff. However, like many other standard recipes, this scheme cannot be used together with nonlocal operators. We have therefore used a mixed approach where we employ pseudopotentials from standard density functionals. For the meta-functional TPSS we used the PBE-derived potential and for the hybrid functionals PBE0, B3LYP, and X3LYP the pseudopotentials from a PBE, BLYP, and XLYP reference are employed. Hartree−Fock calculations are done using pseudopotentials generated from density functional calculations with the Becke exchange functional. The parameters for the pseudopotential generation are the following: Hydrogen atoms are represented by a local pseudopotential with a cutoff of $0.5a_0$ (a_0 is the Bohr radius). The oxygen pseudopotential is of the Kleinman−Bylander form[32] with a nonlocal potential for the s angular momentum and the p angular momentum potential as the local part. The cutoff radii are $1.12a_0$ for both s and p angular momentum channels.

All calculations have been performed with a kinetic energy cutoff of 70 Ry. The screening parameter α in the exact exchange operator was $0.1a_0^{-1}$. The simulation cell for the

liquid-state calculations consisted of 32 molecules at a density of 0.975 g/cm^3. This corresponds to the experimental density at 350 K. After a preequilibration using a classical force field a constant temperature simulation using the BLYP functional was carried out for 10 ps. The final configuration of this simulation was used as a starting point for all trajectories using different functionals. After an equilibration time of 10 ps (5 ps for calculations including exact exchange), averages were taken of the next 10 (5) ps of simulations. The Car−Parrinello method[33] with an electron mass of 600 a.u. was used together with Nosé−Hoover[34−36] chain thermostats of length 4 at 350 K and 0.015 a.u. for the ionic and electronic degrees of freedom. The characteristic frequencies of the thermostats were 2400 and 10 000 cm^{-1}, respectively. The time step for the velocity Verlet integrator was 5 a.u., and calculations were performed using the deuterium mass for hydrogen.

A special version of the CPMD code[37] has been used for all calculations. Simulations with hybrid functionals were performed using a two-way parallelization scheme. Besides the distribution of plane waves, orbital pairs in the exact exchange calculations were distributed over processor groups. The average CPU time per Car−Parrinello molecular dynamics step was 2.8 s on a computer with 576 Itanium2 (1.4 GHz) processors and a QsNet Elan4i communication system. On the same computer system using 36 CPUs, the calculation using a hybrid functional takes 31.2 s, and a pure density functional 0.8 s for a Car−Parrinello molecular dynamics step.

3. Small Water Clusters

We have performed a series of test calculations on the structure and binding energy of the water dimer and cyclic trimer. These calculations allow us to verify the accuracy of our simulation setup and in addition provide information on the performance of different functionals on these small systems showing prototypes of intermolecular interactions that are of importance in the liquid. To assess our simulation setup we compare results with Gaussian basis set calculations using Gaussian03.[38] The plane wave setup that we used has a list of approximations: pseudopotentials, finite plane wave cutoff and reduced cutoff for pair densities, and screened exact exchange. However, the Gaussian basis set used, 6-311++G(3df,2p), in our calculations is not complete, and we can expect errors in structural quantities of about 1 pm (for the oxygen−oxygen distance, see ref 39) and 0.1 kcal/mol for the counterpoise-corrected[40] interaction energy. The counterpoise correction is between 0.2 and 0.4 kcal/mol for the water dimer and between 0.5 and 1.3 kcal/mol for the cyclic trimer (Tables 2 and 3).

For the oxygen−oxygen distance in the water dimer we find consistently larger values for the plane wave calculations. The increase in distance is between 0.5 pm for Hartree−Fock and 4.8 pm for the PBE functional. Part of this difference is due to the not fully converged plane wave cutoff of 70 Ry. Increasing the cutoff results in a shortening of the oxygen−oxygen distance by about 2 pm for the PBE and BLYP functionals. The differences in the averaged trimer oxygen−oxygen distances are smaller (up to 2 pm for B3LYP and Hartree−Fock), and both shorter and longer distances are found. The variation in bond length is below 1 pm for all functionals. The hydrogen bond in the dimer is more linear in the plane wave calculations. Again, we find that a higher plane wave cutoff reduces the difference slightly. Binding energies for the water dimer from the plane wave calculations are within 0.2 kcal/mol of the Gaussian basis set results. Exceptions are the PBE and PBE0 functionals where the differences are 0.36 and 0.28 kcal/mol, respectively. All of the cyclic trimer binding energies are within 0.5 kcal/mol, with the exception of the PBE functional where the difference is 1.22 kcal/mol. However, whereas the binding energy of the dimer was underestimated, the trimer binding energy is overestimated with the plane wave PBE calculation. In summary we can conclude that our setup provides for most functionals an overall accuracy comparable to an extended Gaussian basis set calculation. Slightly larger errors are found for PBE-type functionals (PBE, rPBE, TPSS, and PBE0).

We can get further information about the overall performance of the individual density functionals from the small water cluster calculations in Tables 2 and 3 by comparing to high-level ab initio reference calculations.[41,42] The local density approximation (LDA) drastically overbinds both the dimer and the trimer by almost a factor of 2. Oxygen−oxygen distances are too short by 19 pm in both cases. At the opposite end of the range we find the Hartree−Fock (HF) results. The water dimer is underbound by 1.4 kcal/mol, and the r_{OO} distance is too long by 12 pm. Results for the trimer are even worse with a binding energy of only 10.93 kcal/mol compared to a reference value of 15.90 kcal/mol and an oxygen−oxygen distance that is too long by 17 pm. The revised PBE functional (rPBE) gives slightly better results than HF for the trimer and equally bad results for the dimer. All other functionals show a considerably better performance. The BLYP functional underbinds both the dimer

TABLE 2: Structural Parameters (distances in pm, angles in deg) and Binding Energy E_b (in kcal/mol) for the Water Dimer[a]

	plane waves			6-311++G(3df,2p)		
functional	r_{OO}	α_{OHO}	E_b	r_{OO}	α_{OHO}	E_b
LDA	272.9	168.1	8.61	271.3	168.3	8.85(0.44)
BLYP	297.6	176.6	4.34	296.6	171.8	4.17(0.30)
XLYP	293.0	171.6	4.57	295.3[b]	173.5[b]	4.42[b]
PBE	293.7	177.2	4.56	288.9	172.0	4.92(0.33)
rPBE	303.7	176.8	3.25			
TPSS	293.0	177.3	4.31	289.5[c]	175.1[c]	
B3LYP	294.1	174.8	4.63	293.2	171.7	4.53(0.29)
X3LYP	293.3	171.9	4.96	290.8[b]	174.1[b]	4.97[b]
PBE0	293.6	177.2	4.77	291.6	171.7	5.05(0.36)
HF	303.7	175.1	3.65	303.2	174.7	3.71(0.22)
best ab initio[41]	291.2	174.5	5.02			

[a] Binding energies for Gaussian basis set calculations are counterpoise [40] corrected. The correction energy is given in parentheses. [b] aug-cc-pVTZ(-f) basis from ref 61. [c] From ref 52, enhanced information.

TABLE 3: Structural Parameters (distances in pm) and Binding Energies E_b (in kcal/mol) for the Cyclic Water Trimer[a]

	plane waves		6-311++G(3df,2p)	
functional	$\langle r_{OO} \rangle$	E_b	$\langle r_{OO} \rangle$	E_b
LDA	259	29.80	258	29.66(1.31)
BLYP	284	13.67	284	13.20(0.88)
XLYP	284	14.12		
PBE	276	16.69	277	15.47(0.94)
rPBE	289	11.65		
TPSS	275	15.55		
B3LYP	283	14.24	281	14.20(0.81)
X3LYP	280	15.39		15.52[b]
PBE0	277	16.61	278	16.06(1.04)
HF	295	10.93	293	11.07(0.58)
MP2[42] (extrapolated)	278	15.90		

[a] Binding energies for Gaussian basis set calculations are counterpoise-corrected.[40] The correction energy is given in parentheses. Oxygen−oxygen distances vary by less than 1 pm for all functionals tested. Averaged values are given in the table. [b] aug-cc-pVTZ(-f) basis from ref 62.

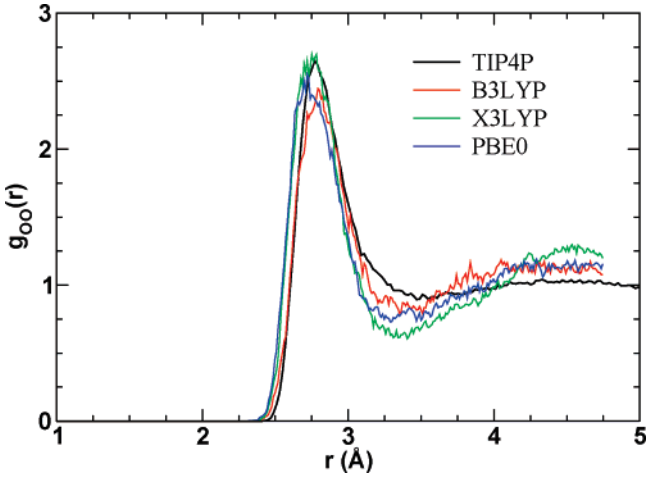

Figure 1. Partial oxygen−oxygen radial distribution function calculated for the TIP4P force field and three hybrid functionals.

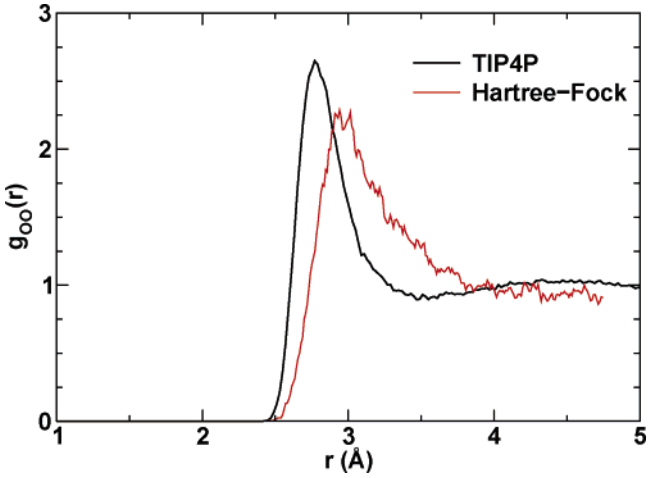

Figure 2. Partial oxygen−oxygen radial distribution function calculated for the TIP4P force field and Hartree−Fock.

and the trimer more than other functionals with approximate exchange and correlation. The hybrid functionals outperform the pure density functionals and are closest to the high-level quantum chemical calculations.

4. Liquid Water

The simulation box of length 9.939 Å containing 32 water molecules corresponds to the experimental density of water at atmospheric pressure and 350 K temperature. This model was chosen due to computational time constraints. It also coincides with the number of molecules used in earlier simulations of liquid water.[15,16] More recent simulations were able to treat larger samples.[8,9,11,13] Although small differences were found, no important size effect in structural and dynamical properties was reported. For computational reasons the plane wave cutoff has been chosen to be 70 Ry in accordance with earlier simulations, lying at the lower end of the acceptable convergence range. To minimize problems with slow time scales[13,14] we chose a simulation temperature of 350 K. The TIP4P force field[43] was used to generate reference partial radial distribution functions. This model is believed to give results close to experimental values.[44]

In Figure 1 the oxygen−oxygen radial distribution function (RDF) of the TIP4P reference is shown together with the results from the simulations using the hybrid functionals B3LYP, X3LYP, and PBE0. Results are in good agreement for position and height of the first peak. The maximum for the X3LYP and PBE0 simulations is at slightly smaller distances (2−4 pm), and the peak height for B3LYP and PBE0 is smaller by about 0.2 units. All hybrid functionals show a more pronounced minimum after the first peak and signature of a second shell than the TIP4P reference. These results can be put into perspective by comparison to the simulation using the Hartree−Fock method presented in Figure 2. The Hartree−Fock method fails to reproduce the position and height of the first peak and shows no signature of a second solvation shell. Similar results to our findings for the B3LYP functional and the Hartree−Fock method were recently reported by Xenides et al.[45] using a QM/MM approach and small basis sets.

In Table 4 the characteristics of the oxygen−oxygen RDF are compared for the full series of functionals used in this study. For the position and height of the first peak we also give an estimate for the statistical accuracy. These estimates correspond to the maximum deviations of the values collected from a series of samples evaluated from a sliding window of half of the total sampling period. However, the rather short duration of the simulations only allow a rough estimate of the statistical error by this method. The results obtained for the common DFT functionals BLYP and PBE and the meta-functional TPSS are in accordance with previous publications.[8,13,14] Together with the XLYP functional, they have in common that the oxygen−oxygen RDF is slightly overstructured. The hybrid functionals show a good agreement for position, height, and width of the first peak compared to the TIP4P reference whereas the first minimum is at slightly smaller distances and has a lower value. However, also with respect to these structural parameters all hybrid functionals are closer to the reference than the pure density functionals. We have to point out that all gradient-corrected functionals perform much better than the Hartree−Fock method and the extremely overbinding LDA. The rPBE functional is a special case. The change of a single parameter in the exchange functional leads to a drastic change in hydrogen bonding. As can be seen already in the structural and energetic results for the dimer and the trimer, much weaker hydrogen bonds are predicted, leading to a slightly understructured RDF. This behavior was already noted in earlier simulations.[11,24]

TABLE 4: Position, Height, and Full Width at Half-Maximum (fwhm) Height of the First Peak of the Partial Oxygen−Oxygen Radial Distribution Function for Different Density Functionals[a]

functional	r_{max}	$g_{OO}(r_{max})$	fwhm	r_{min}	$g_{OO}(r_{min})$
LDA	259(2)	5.07(0.07)	21	312	0.23
BLYP	279(4)	3.00(0.20)	37	331	0.48
XLYP	277(2)	3.21(0.11)	34	332	0.40
PBE	270(5)	2.99(0.08)	37	329	0.47
rPBE	281(2)	2.29(0.09)	47	334	0.80
TPSS	271(2)	3.40(0.05)	32	329	0.33
B3LYP	279(2)	2.48(0.10)	45	340	0.81
X3LYP	276(6)	2.75(0.10)	40	336	0.62
PBE0	274(6)	2.58(0.08)	44	335	0.73
HF	297(6)	2.35(0.13)	78		
TIP4P	278	2.64	44	352	0.90

[a] Values in parentheses are maximum deviations over the sampling period, calculated from a sliding window of half width. Values are given in picometers.

The oxygen−hydrogen and hydrogen−hydrogen RDFs (Figures 3 and 4) for hybrid functionals tested are in agreement with the reference function. The first intermolecular oxygen−hydrogen peak for X3LYP and PBE0 is at a slightly smaller distance, and the minimum at about 2.5 Å is more pronounced for all hybrid functionals. Very similar results can be seen in

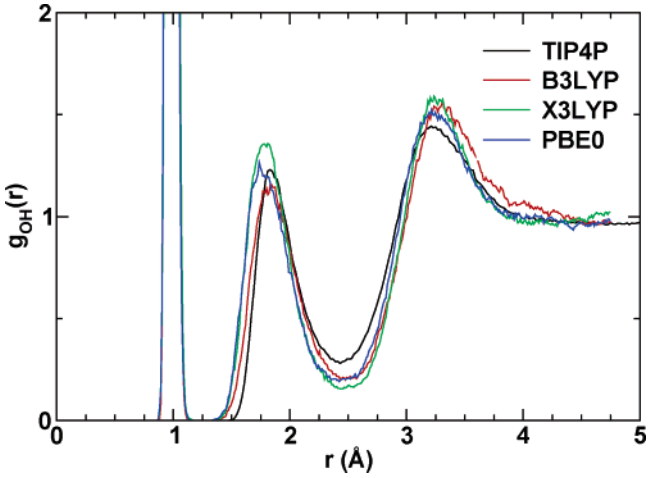

Figure 3. Partial oxygen−hydrogen radial distribution function calculated for the TIP4P force field and three hybrid functionals. The intramolecular peak for the TIP4P force field has been omitted.

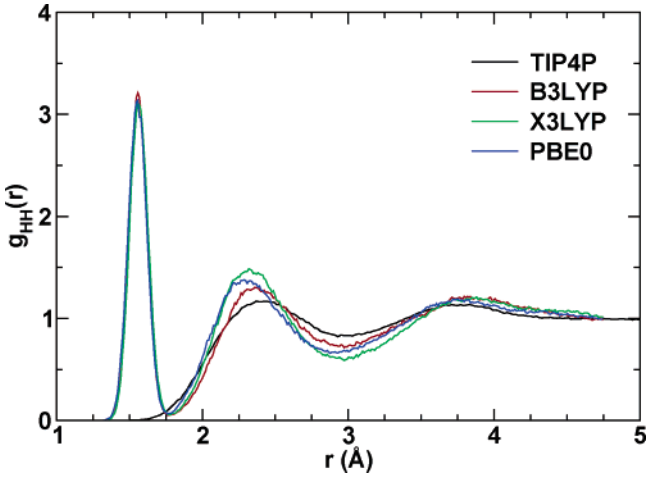

Figure 4. Partial hydrogen−hydrogen radial distribution function calculated for the TIP4P force field and three hybrid functionals. The intramolecular peak for the TIP4P force field has been omitted.

TABLE 5: Self-Diffusion Coefficient *D* Calculated for Different Density Functionals

functional	D (Å^2/ps)
LDA	0.013
BLYP	0.048
XLYP	0.028
PBE	0.047
rPBE	0.18
TPSS	0.032
B3LYP	0.30
X3LYP	0.17
PBE0	0.28
HF	0.47
experiment[46] (45 °C)	0.2979

the hydrogen−hydrogen intermolecular peak in Figure 4. The first peak is higher by 0.2−0.3 units and at a smaller distance.

The experimental value of the self-diffusion coefficient D for heavy water at 45 °C is 0.2979 Å^2/ps.[46] When the experimental values were extrapolated to 77 °C, the temperature used in this study, we obtain a value close to 0.5 Å^2/ps. The length of the simulations in this study does not allow us to determine the self-diffusion coefficient accurately. However, we can see in the values collected in Table 5 the same trends as in the RDFs. The pure gradient-corrected density functionals show a very low diffusivity of 0.03−0.05 Å^2/ps. The value for the local density functional is even lower, at 0.013 Å^2/ps. For the hybrid functionals we find considerably higher values (0.17−0.30 Å^2/ps), although still below the estimated experimental value. Hartree−Fock theory shows the highest diffusivity (0.47 Å^2/ps), and for the revised PBE functional the value is relatively high (0.18 Å^2/ps) as well. Thus the hybrid functionals, B3LYP, X3LYP, and PBE0, are the only functionals studied here that are able to provide both good structural values (RDFs) and dynamical behavior (self-diffusion coefficient D). To what extent the calculated self-diffusion coefficients for the hybrid functionals agree with experimental values is difficult to assess. Besides the problems of short simulation times, noncomplete basis sets, and finite size effects, there is also the uncertainty of quantum effects.[20]

TABLE 6: Distribution of the Number of Hydrogen Bonds for Different Density Functionals[a]

	number of hydrogen bonds					
functional	1	2	3	4	5	average
LDA	0	3	16	75	6	3.84
BLYP	0	6	19	66	7	3.68
XLYP	0	6	19	69	6	3.75
PBE	0	6	24	66	6	3.78
rPBE	1	11	33	51	6	3.56
TPSS	0	4	20	71	6	3.82
B3LYP	0	6	27	61	6	3.67
X3LYP	0	6	34	51	8	3.58
PBE0	0	11	26	57	4	3.48
HF	3	11	40	39	6	3.31

[a] The values given are percentages of molecules with the given number of hydrogen bonds. Hydrogen bonds are defined by a geometrical criteria. The oxygen−oxygen distance is smaller than 3.5 Å, and the O−H−O angle is larger than 135°.

Another interesting structural quantity with direct impact on the self-diffusion is the average number of hydrogen bonds in which a molecule is involved. This quantity cannot be directly measured but has been inferred from experiments.[47] In Table 6 the percentages of molecules with a given number of hydrogen bonds are listed. A geometrical definition of a hydrogen bond was used: All molecular pairs with an oxygen−oxygen distance of less than 3.5 Å and an O−H−O angle of more than 135° are counted as hydrogen bonds. The Hartree−Fock method shows an almost equal percentage of molecules with three and four hydrogen bonds, and also molecules with only one and two bonds are rather frequently encountered. At the opposite end we find the LDA with 75% four-bonded molecules. Gradient-corrected pure density functionals (with the exception of rPBE) show the clear dominance of the fourfold case (66−71%) and only few twofold cases (6%). The hybrid functionals have a more equal distribution between the three- and fourfold-bonded cases, namely, a 1:2 ratio compared to a 1:3 ratio. The percentage of molecules with lower (one and two) or higher (five) numbers of bonds is for all functionals very similar. The average number of hydrogen bonds (Table 6) is between 3.68 (BLYP) and 3.78 (PBE) for the standard density functionals and 3.48 (PBE0), 3.58 (X3LYP), and 3.67 (B3LYP) for the hybrid functionals. These values can be compared with an experimental[47] estimate of 3.58 at 300 K. It is also interesting to investigate the type of hydrogen bonds, donors or acceptors, that are involved in the case of the threefold-bonded molecules. We find that for the hybrid functionals the ratio between double donor−single acceptor (2D1A) to single donor−double acceptor (1D2A) is 2D1A/1D2A = 58/42 for B3LYP and PBE0 and 64:36 for X3LYP. For BLYP and XLYP the ratios are 72/28 and 67/33. For the PBE functional we find a 67/33 ratio.

The calculation of molecular dipole moments is an interesting analysis tool in first-principles molecular dynamics simulations

TABLE 7: Maximum Value and Full Width at Half-Maximum (fwhm) Height of the Molecular Dipole Distribution for Different Density Functionals[a]

functional	dipole	fwhm
LDA	3.82	1.12
BLYP	3.10	0.65
XLYP	3.12	0.66
PBE	3.27	0.78
rPBE	2.91	0.72
TPSS	3.19	0.70
B3LYP	2.91	0.65
X3LYP	3.07	0.69
PBE0	2.99	0.67
HF	2.58	0.45

[a] All values are given in Debye units.

of molecular liquids.[48] In all simulations maximally localized Wannier functions[49,50] were calculated every 0.6 fs along the trajectories using the method described by Kirchner and Hutter.[51] From the centers of the Wannier functions we calculated the molecular dipole distribution for the different functionals. The average dipole and the full width at half-maximum height (fwhm) of these distributions are listed in Table 7. Except for the HF method, which shows a lower average dipole (2.58 D) and a smaller distribution (0.45 D), and the local density approximation, which has a larger average dipole (3.82 D) and a larger distribution (1.12 D), the results are similar for all density functionals, especially the distribution of the dipoles, as represented by the fwhm value, which varies only between 0.65 and 0.78 D. The average value of the molecular dipoles for the pure density functionals is slightly higher (between 3.10 and 3.27 D) than those for the hybrid functionals (2.91, 2.99, and 3.07 D).

5. Summary and Conclusions

We have studied the structural and dynamic properties of liquid water using plane wave basis sets in first-principles molecular dynamics simulations. We have included hybrid density functionals in the study and compared their performance together with other standard exchange and correlation functionals. We have first demonstrated in small water molecules that our implementation is accurate and consistent with all-electron calculations establishing a precedence to proceed with an examination of the liquid state of water.

We find improved results with the three tested hybrid functionals compared to those from local and semilocal, gradient-based functionals or Hartree−Fock calculations. We quantified the structural accuracy with the height and width of the oxygen−oxygen pair correlation function and the dynamic properties with the self-diffusion coefficient. Both of them agree better with experimental values, albeit the MSDs are still somewhat slower than the currently accepted experimental results. Thus, the overall accuracy of the hybrid functionals known from static calculations[52,53] seems to transfer to the dynamical properties. The average number of hydrogen bonds per molecule using the hybrid functionals is slightly smaller than predicted by the standard GGA functionals. Molecular dipole moments are slightly smaller, reducing the gap to the values of empirical force fields. The limited range and accuracy of our simulations do not allow us to assess the relative performance of the hybrid functionals. However, the consistency of the results of the three hybrid functionals is remarkable.

For structural properties such as the RDF, we have demonstrated that the insufficient accuracy in the description of the electronic structure seems to play a dominant role. Although we cannot rule out the importance of nuclear quantum effects, there are indications that these effects are small.[20] The time and length scale of the simulations can be systematically studied and improved upon by increasing computing power and further developing the algorithm of the current implementation. Thus, this work is a further contribution on the way to the reproduction and subsequent understanding of the mysteries of water via first-principles simulations.

Acknowledgment. Part of this work was performed under the auspices of the U. S. Department of Energy by the University of California Lawrence Livermore National Laboratory under Contract No. W-7405-End-48. Calculations were performed on the computer systems of LLNL's M&IC computing resources (MRC and Thunder), CSCS in Manno and the Matterhorn Cluster at the University of Zurich.

References and Notes

(1) Stillinger, F. H. *Science* **1980**, *209*, 451.
(2) Guillot, B. *J. Mol. Liq.* **2002**, *101*, 219.
(3) Kohn, W.; Sham, L. J. *Phys. Rev.* **1965**, *140* (4A), A1133−A1139.
(4) Becke, A. D. *Phys. Rev. A* **1988**, *38* (6), 3098−3100.
(5) Lee, C. T.; Yang, W. T.; Parr, R. G. *Phys. Rev. B* **1988**, *37* (2), 785−789.
(6) Perdew, J. P.; Burke, K.; Ernzerhof, M. *Phys. Rev. Lett.* **1996**, *77* (18), 3865−3868.
(7) Kuo, I.-F. W.; Mundy, C. J. *Science* **2004**, *303*, 658−660.
(8) Kuo, I.-F. W.; Mundy, C. J.; McGrath, M. J.; Siepmann, J. I.; VandeVondele, J.; Sprik, M.; Hutter, J.; Chen, B.; Klein, M. L.; Mohamed, F.; Krack, M.; Parrinello, M. *J. Phys. Chem. B* **2004**, *108* (34), 12990−12998.
(9) Grossman, J. C.; Schwegler, E.; Draeger, E. W.; Gygi, F.; Galli, G. *J. Chem. Phys.* **2004**, *120*, 300−311.
(10) Schwegler, E.; Grossman, J. C.; Gygi, F.; Galli, G. *J. Chem. Phys.* **2004**, *121*, 5400−5409.
(11) Fernandez-Serra, M. V.; Artacho, E. *J. Chem. Phys.* **2004**, *121*, 11136−11144.
(12) Mantz, Y. A.; Chen, B.; Martyna, G. J. *Chem. Phys. Lett.* **2005**, *405*, 294−299.
(13) Sit, P. H. L.; Marzari, N. *J. Chem. Phys.* **2005**, *122*, 204510.
(14) VandeVondele, J.; Mohamed, F.; Krack, M.; Hutter, J.; Sprik, M.; Parrinello, M. *J. Chem. Phys.* **2005**, *122*, 014515.
(15) Laasonen, K.; Sprik, M.; Parrinello, M.; Car, R. *J. Chem. Phys.* **1993**, *99*, 9080−9089.
(16) Sprik, M.; Hutter, J.; Parrinello, M. *J. Chem. Phys.* **1996**, *105*, 1142−1152.
(17) McGrath, M. J.; Siepmann, J. I.; Kuo, I.-F. W.; Mundy, C. J.; VandeVondele, J.; Sprik, M.; Hutter, J.; Mohamed, F.; Krack, M.; Parrinello, M. *Comput. Phys. Commun.* **2005**, *169* (1−3), 289−294.
(18) McGrath, M. J.; Siepmann, J. I.; Kuo, I.-F. W.; Mundy, C. J.; VandeVondele, J.; Hutter, J.; Mohamed, F.; Krack, M. *ChemPhysChem* **2005**, *6*, 1894.
(19) McGrath, M. J.; Siepmann, J. I.; Kuo, I.-F. W.; Mundy, C. J.; VandeVondele, J.; Hutter, J.; Mohamed, F.; Krack, M. *J. Phys. Chem. A* **2006**, *110*, 640−646. 2005 ASAP, http://dx.doi.org/10.1021/jp0535947.
(20) Chen, B.; Ivanov, I.; Klein, M. L.; Parrinello, M. *Phys. Rev. Lett.* **2003**, *91*, 215503.
(21) Wernet, P.; Nordlund, D.; Bergmann, U.; Cavalleri, M.; Odelius, M.; Ogasawara, H.; Näslund, L. Å.; Hirsch, T. K.; Ojamäe, L.; Glatzel, P.; Pettersson, L. G. M.; Nilsson, A. *Science* **2004**, *304*, 995−999.
(22) Smith, J. D.; Cappa, C. D.; Wilson, K. R.; Messer, B. M.; Cohen, R. C.; Saykally, R. J. *Science* **2004**, *306*, 851−853.
(23) Näslund, L. Å.; Luning, J.; Ufuktepe, Y.; Ogasawara, H.; Wernet, P.; Bergmann, U.; Pettersson, L. G. M.; Nilsson, A. *J. Phys. Chem. B* **2005**, *109*, 13835−13839.
(24) Asthagiri, D.; Pratt, L. R.; Kress, J. D. *Phys. Rev. E* **2003**, *68*, 041505.
(25) Gygi, F.; Baldereschi, A. *Phys. Rev. B* **1986**, *34*, 4405−4408.
(26) Chawla, S.; Voth, G. A. *J. Chem. Phys.* **1998**, *108*, 4697−4700.
(27) Marx, D.; Hutter, J. In *Modern Methods and Algorithms of Quantum Chemistry*; Grotendorst, J., Ed.; NIC Series 1; FZ Jülich: Jülich, Germany, 2000; pp 329−477.
(28) Paier, J.; Hirschl, R.; Marsman, M.; Kresse, G. *J. Chem. Phys.* **2005**, *122*, 234102.
(29) Bernasconi, L.; Sprik, M.; Hutter, J. *Chem. Phys. Lett.* **2004**, *394*, 141−146.
(30) Heyd, J.; Scuseria, G. E.; Ernzerhof, M. *J. Chem. Phys.* **2003**, *118*, 8207−8215.

(31) Troullier, N.; Martins, J. L. *Phys. Rev. B* **1991**, *43* (3), 1993−2006.
(32) Kleinman, L.; Bylander, D. M. *Phys. Rev. Lett.* **1982**, *48*, 1425−1428.
(33) Car, R.; Parrinello, M. *Phys. Rev. Lett.* **1985**, *55*, 2471.
(34) Nosé, S. *J. Chem. Phys.* **1984**, *81*, 511−519.
(35) Hoover, W. G. *Phys. Rev. A* **1985**, *31*, 1695−1697.
(36) Martyna, G. J.; Klein, M. L.; Tuckerman, M. E. *J. Chem. Phys.* **1992**, *97*, 2635−2643.
(37) *CPMD*, version 3.9; IBM Corp., MPI für Festkörperforschung: Stuttgart, Germany, 1990−2004, 1997−2001. http://www.cpmd.org/.
(38) Frisch, M. J.; Trucks, G. W.; Schlegel, H. B.; Scuseria, G. E.; Robb, M. A.; Cheeseman, J. R.; Montgomery, J. A., Jr.; Vreven, T.; Kudin, K. N.; Burant, J. C.; Millam, J. M.; Iyengar, S. S.; Tomasi, J.; Barone, V.; Mennucci, B.; Cossi, M.; Scalmani, G.; Rega, N.; Petersson, G. A.; Nakatsuji, H.; Hada, M.; Ehara, M.; Toyota, K.; Fukuda, R.; Hasegawa, J.; Ishida, M.; Nakajima, T.; Honda, Y.; Kitao, O.; Nakai, H.; Klene, M.; Li, X.; Knox, J. E.; Hratchian, H. P.; Cross, J. B.; Bakken, V.; Adamo, C.; Jaramillo, J.; Gomperts, R.; Stratmann, R. E.; Yazyev, O.; Austin, A. J.; Cammi, R.; Pomelli, C.; Ochterski, J. W.; Ayala, P. Y.; Morokuma, K.; Voth, G. A.; Salvador, P.; Dannenberg, J. J.; Zakrzewski, V. G.; Dapprich, S.; Daniels, A. D.; Strain, M. C.; Farkas, O.; Malick, D. K.; Rabuck, A. D.; Raghavachari, K.; Foresman, J. B.; Ortiz, J. V.; Cui, Q.; Baboul, A. G.; Clifford, S.; Cioslowski, J.; Stefanov, B. B.; Liu, G.; Liashenko, A.; Piskorz, P.; Komaromi, I.; Martin, R. L.; Fox, D. J.; Keith, T.; Al-Laham, M. A.; Peng, C. Y.; Nanayakkara, A.; Challacombe, M.; Gill, P. M. W.; Johnson, B.; Chen, W.; Wong, M. W.; Gonzalez, C.; Pople, J. A. *Gaussian 03*, revision C.02; Gaussian, Inc.: Wallingford, CT, 2004.
(39) Koch, W.; Holthausen, M. C. *A Chemist's Guide to Density Functional Theory*, 2nd ed.; Wiley-VCH: New York, 2002.
(40) Boys, S. F.; Bernardi, F. *Mol. Phys.* **1970**, *19* (*4*), 553−566.
(41) Klopper, W.; van Duijneveldt-van de Rijdt, J. G. C. M.; van Duijneveldt, F. B. *Phys. Chem. Chem. Phys.* **2000**, *2* (10), 2227−2234.
(42) Nielsen, I. M. B.; Seidl, E. T.; Janssen, C. L. *J. Chem. Phys.* **1999**, *110* (19), 9435−9442.
(43) Jorgensen, W. L.; Chandrasekhar, J.; Madura, J. D.; Impey, R. W.; Klein, M. L. *J. Chem. Phys.* **1983**, *79* (2), 926−935.
(44) Hura, G.; Russo, D.; Glaeser, R. M.; Head-Gordon, T.; Krack, M.; Parrinello, M. *Phys. Chem. Chem. Phys.* **2003**, *5*, 1981−1991.
(45) Xenides, D.; Randolf, B. R.; Rode, B. M. *J. Chem. Phys.* **2005**, *122*, 174506.
(46) Mills, R. *J. Phys. Chem.* **1973**, *77*, 685−688.
(47) Soper, A. K.; Bruni, F.; Ricci, M. A. *J. Chem. Phys.* **1997**, *106*, 247.
(48) Silvestrelli, P. L.; Parrinello, M. *J. Chem. Phys.* **1999**, *111*, 3572−3580.
(49) Marzari, N.; Vanderbilt, D. *Phys. Rev. B* **1997**, *56*, 12847−12865.
(50) Berghold, G.; Mundy, C. J.; Romero, A. H.; Hutter, J.; Parrinello, M. *Phys. Rev. B* **2000**, *61*, 10040−10048.
(51) Kirchner, B.; Hutter, J. *J. Chem. Phys.* **2004**, *121*, 5133−5142.
(52) Staroverov, V. N.; Scuseria, G. E.; Tao, J. M.; Perdew, J. P. *J. Chem. Phys.* **2003**, *119* (23), 12129−12137.
(53) Xu, X.; Goddard III, W. A. *Proc. Natl. Acad. Sci. U.S.A.* **2004**, *101* (9), 2673−2677.
(54) Becke, A. D. *J. Chem. Phys.* **1993**, *98*, 5648−5652.
(55) Adamo, C.; Barone, V. *J. Chem. Phys.* **1999**, *110*, 6158−6170.
(56) Goedecker, S.; Teter, M.; Hutter, J. *Phys. Rev. B* **1996**, *54* (3), 1703−1710.
(57) Wang, Y.; Perdew, J. P. *Phys. Rev. B* **1991**, *44*, 13298−13307.
(58) Zhang, Y.; Yang, W. *Phys. Rev. Lett.* **1998**, *80*, 890.
(59) Perdew, J. P.; Zunger, A. *Phys. Rev. B* **1981**, *23*, 5048.
(60) Tao, J. M.; Perdew, J. P.; Staroverov, V. N.; Scuseria, G. E. *Phys. Rev. Lett.* **2003**, *91* (212), 146401−1.
(61) Xu, X.; Goddard III, W. A. *J. Phys. Chem. B* **2004**, *108* (12), 2305−2313.
(62) Su, J. T.; Xu, X.; Goddard, W. A., III *J. Phys. Chem. A* **2004**, *108*, 10518−10526.